CHAPTER 9

DYNAMICS OF SUPERPLUMES IN THE LOWER MANTLE

DAVID A. YUEN[1], MARC MONNEREAU[2], ULRICH HANSEN[3], MASANORI KAMEYAMA[4], AND CTIRAD MATYSKA[5]

[1] *Department of Geology and Geophysics and Minnesota Supercomputing Institute, University of Minnesota, Minneapolis 55455, USA;*
E-mail: daveyuen@gmail.com

[2] *UMR 5562, CNRS—Universiteté Paul Sabatier Toulouse III, 14 Avenue E. Belin, 31400 Toulouse, France*

[3] *Institut für Geophysik, University of Münster, 48149 Münster, Germany*

[4] *Earth Simulator Center, JAMSTEC, Kanazawa-ku, 237-0061 Yokohama, Japan*

[5] *Department of Geophysics, Faculty of Mathematics and Physics, Charles University, 180 00 Prague 8, Czech Republic*

Abstract
Superplumes in the lower mantle have been inferred for a long time by the presence of two very large provinces with slow seismic wave velocities. These extensive structures are not expected from numerical and laboratory experiments nor are they found in thermal convection with constant physical properties under high Rayleigh number conditions. Here we summarize our dynamical understanding of superplume structures within the framework of thermal convection. The numerical studies involve both two- and three-dimensional models in Cartesian and spherical-shell geometries. The theoretical approach is based on models with increasing complexity, starting with the incompressible Boussinesq model and culminating with the anelastic compressible formulation. We focus here on the (1) depth-dependence of variable viscosity and thermal coefficient of expansion (2) radiative thermal conductivity and (3) both upper- and deep-mantle phase transitions. All these physical factors in thermal convection help to create conditions favorable for the formation of partially-layered convection and large-scale upwelling structures in the lower mantle.

1 INTRODUCTION

The notion of superplumes or large-scale structures in the lower mantle has been around for more than twenty years, since the initial tomographic pictures shown by Dziewonski (1984). The surface manifestation of this seismic anomaly was

D. A. Yuen et al. (eds.), Superplumes, 239–268.
© 2007 *Springer.*

recognized and associated with the South Pacific Superswell, which is known as a broad area of shallow seafloor under French Polynesia (McNutt and Judge, 1990). This tantalizing concept, which ran counter to the idea of narrow conduit-like plumes in the deep mantle, proposed earlier by Morgan (1971), has stood the scrutiny of many subsequent tomographic models. So there has now emerged a picture in the lower mantle consisting of two regions with prominent slow seismic velocities, which extend from the core-mantle boundary up to around 1000 km in depth (Su and Dziewonski, 1992; Masters et al., 2000; Li and Romanowicz, 1996; Grand et al., 1997; Zhao, 2001, 2004; Montelli et al., 2004).

These structures have also been interpreted in terms of clusters of plumes (Schubert et al., 2004), arising from plume-plume collisions (Vincent and Yuen, 1988). Maruyama (1994) has discussed the geological and geophysical ramifications of superplumes in mantle evolution and coined the term "plume tectonics" which predicts that eventually these superplumes would control the upper-mantle circulation. Since that time the interest in superplumes has grown immensely, as evidenced by the numerous conferences and a big thirst is fast building up for understanding this interesting phenomenon from physical and geological standpoints.

The appearance of these few obese plumes in the lower mantle can shed light on the physical properties of the lower mantle and indicates that the mantle viscosity cannot be constant throughout the mantle, as the initial work by Hansen et al. (1993) showed a dramatic reduction in the population of lower-mantle plumes with the introduction of depth-dependent thermal expansivity and viscosity. This work was then followed up by Van Keken and Yuen (1995) and Yuen et al. (1996), who emphasized the importance of a high viscosity region in the deep mantle. Davies (2005) has shown that downwellings in the presence of depth-dependent viscosity can induce a few number of plumes in 3-D spherical-shell convection at high Rayleigh numbers. Superplumes can also be considered from the point of view of thermal-chemical convection, as first pointed out by Yuen et al. (1993) from arguments based on the magnitude of seismic velocity anomalies and depth dependence of equation of state parameters in the lower mantle. This phenomenon of accumulation of chemical anomalies in the lower mantle has been corroborated (e.g., Trampert et al., 2004) and investigated numerically by Hansen and Yuen (1989), Tackley (1998), Mc Namara and Zhong (2004) and experimentally by Davaille (1999) and Davaille et al. (2005). Changes in transport properties, such as radiative thermal conductivity (Matyska et al., 1994; Dubuffet and Yuen, 2000; Matyska and Yuen, 2005) and grain-size dependent rheology (Korenaga, 2005) may also broaden lower-mantle plumes considerably.

Although thermal-chemical convection takes place to some degree in the mantle (e.g., Trampert et al., 2004), in this chapter we will direct our attention to thermal convection, because this represents a legitimate end member and we can understand from these exercises a great deal concerning the interaction between the transport properties and phase transitions in nonlinear thermal convection, already a complicated enough phenomenon. Having stated this caveat, we will therefore discuss our results only within the framework of thermal convection.

We will begin in section 2 with a description of our models, which include both two- and three-dimensional models and also have both Cartesian and spherical geometries. We will focus on the influences of variable viscosities, radiative thermal conductivity and phase transitions, which also includes the recently discovered post-perovskite phase transition (Murakami et al., 2004). Section 3 will display the results from these models. Finally we give the conclusions and present our perspectives.

2 MODELS AND FORMULATION

Within our theoretical framework we will employ the viscous fluid model for describing lower-mantle convection and neglect the effects of viscoelasticity (e.g., Mühlhaus and Regenauer-Lieb, 2005) and plasticity (Kameyama et al., 1999; Regenauer-Lieb and Yuen, 2003), which are important for plate dynamics. The conservation equations of mantle convection in this viscous regime can be found in many places, e.g. (Schubert et al., 2002). We will just highlight the salient points here. For the Earth's mantle the conservation of mass is governed by the following dimensionless elliptic partial differential equation in the short-time limit of neglecting elastic waves:

$$\nabla \cdot (\rho \underset{\sim}{\mathbf{V}}) = 0, \tag{1}$$

where ρ is density field non-dimensionalized by the surface density, and $\underset{\sim}{\mathbf{V}}$ is the velocity vector, non-dimensionalized by K/h, where K is the surface thermal diffusivity and h is the mantle thickness. Conservation of mass, as expressed by eqn. (1), is called the anelastic compressible approximation, where ρ, the density depends on the pressure or depth. Within the framework of the incompressible or Boussinesq approximation ρ is taken to be a constant and eqn. (1) becomes $\nabla \cdot \underset{\sim}{\mathbf{V}} = 0$. We note that the Boussinesq approximation is adequate for the upper-mantle, but may be deficient for lower-mantle dynamics, because of the influence of equation of state (see Tan and Gurnis, 2005).

The conservation of momentum for the Earth's mantle does not include either the influences of inertia or rotation because of its high viscosity and just expresses a balance among the viscous stresses, buoyancy and pressure gradient. It is given in non-dimensional form by the elliptic partial differential equation for

$$\nabla \cdot \underset{\approx}{\tau}(\underset{\sim}{\mathbf{V}}) + \mathrm{Ra}\alpha\theta \mathrm{e}_z - \nabla\pi = 0, \tag{2}$$

where $\underset{\approx}{\tau}$ is the Cauchy stress tensor given by the mathematical relationship between $\underset{\approx}{\tau}$ and the spatial derivatives of the velocity field. This relationship belongs to the field of mantle rheology (Ranalli, 1995). The dynamical pressure is given by π. α is thermal expansion coefficient, which can be depth-dependent, θ is the temperature perturbation rendered dimensionless by the temperature drop across the mantle (van den Berg and Yuen, 1998) and Ra is the dimensionless Rayleigh number which measures the vigor of convection.

For the Earth's mantle the spatially averaged Rayleigh number lies between 10^6 and 10^7. The constitutive relationship between the deviatoric stress tensor σ and the velocity is given for Newtonian fluids by:

$$\underset{\sim}{\sigma} = \eta(\mathrm{T}, p, \ldots)\left(\nabla \underset{\sim}{\mathbf{v}} + (\nabla \underset{\sim}{\mathbf{v}})^{\mathrm{T}}\right), \tag{3}$$

where η is called the dynamic viscosity and this particular transport coefficient for momentum depends on the absolute temperature T, the hydrostatic pressure p and other variables, such as grain-size (Solomatov, 1996) and volatile content (Hirth and Kohlstedt, 1996).

The transfer of heat in the mantle is governed by the following dimensionless nonlinear partial differential equation, which has the only time-dependence for thermal convection involving viscous fluids,

$$\rho \frac{\partial \mathrm{T}}{\partial t} = \nabla \cdot (\mathrm{K} \nabla \mathrm{T}) - \rho \underset{\sim}{\mathbf{v}} \cdot \nabla \mathrm{T} - D\alpha w\,(\mathrm{T} + \mathrm{T}_0) + \left(\frac{\mathrm{D}}{\mathrm{Ra}}\right)(\underset{\sim}{\sigma} : \nabla \underset{\sim}{\mathbf{v}}) + R, \tag{4}$$

where T is the dimensionless temperature, w is the vertical velocity, t is time nondimensionalized by the thermal diffusion time across the whole mantle, K is the thermal diffusivity which depends on temperature and pressure (Hofmeister, 1999), R is the dimensionless internal heating rate (e.g., Leitch and Yuen, 1989), T_0 is the temperature of the viscous surface (see Steinbach and Yuen, 1998), D is the dissipation number (Christensen and Yuen, 1985), given by α h/(g Cp), where Cp is the specific heat at constant pressure, g is the gravitational acceleration. In this paper we assume Cp to be a constant, since the mantle temperature is well above the Debye temperature.

The parameters in D appearing in (4) assume the magnitude of the surface values. The energy equation, as expressed above, includes mechanical heating from adiabatic work and viscous heating, as manifested by the dissipation number, which depends on the equation of state. In the Boussinesq approximation the dissipation number is zero and there is no irreversible production of heat from fluid motions. In the extended Boussinesq framework (Christensen and Yuen, 1985), D is non-zero in the energy equation but the continuity equation takes the incompressible limit with a constant density field. For additional details of the non-dimensionalized equations, the reader is referred to Matyska and Yuen (2007).

The two transport properties, η and K, hold the key to the style of mantle convection. The temperature-dependence of mantle viscosity is important for the style of surface deformation because of the sharp variations of viscosity associated with the top thermal boundary layer. In contrast, the variations in the magnitude of temperature-dependence of thermal diffusivity are much smaller than those associated with viscosity, but because K appears in the time-dependent equation governing mantle convection, this positioning of K in the master equation (e.g., Haken, 1983) of the mantle convection system enables it to exert much more subtle influence on mantle convection, which depends on the nature of the heat-transfer mechanism, whether it is lattice conductivity (Yanagawa et al., 2005) or radiative conductivity

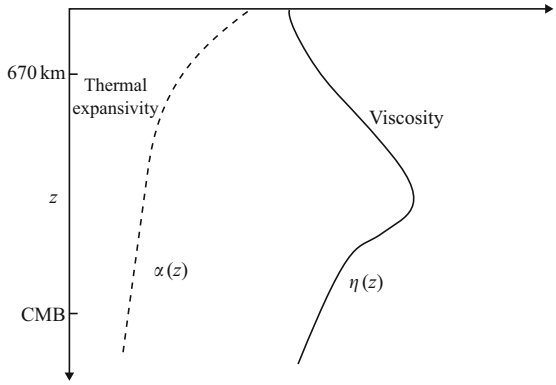


Figure 1. The depth-dependent trends of the coefficient of thermal expansion α and of viscosity η in the mantle. The viscosity profile is taken from the work of Forte and Mitrovica (2001) and Mitrovica and Forte (2004). This viscosity peak in the mid lower-mantle was first shown by Ricard and Wuming (1991). The pressure dependence of α has now been extended to perovskite in the lower mantle (Katsura et al., 2005).

(Dubuffet et al., 2002). In contrast, the viscosity appears as a coefficient in the elliptic equation. Variations in the viscosity with a much larger magnitude are needed to produce significant effects in mantle convection. The depth dependence of α and η stabilizes mantle convection (Hansen et al., 1993) and induces the formation of fewer upwellings. Their general appearances are sketched in Figure 1. We note that α for mantle materials decreases with pressure, which means the potency of thermal buoyancy becomes much weaker in the deep mantle, leading to the situation of dominance by compositional effects (Schott et al., 2002). The pressure-dependence of mantle viscosity depends sensitively on the creep mechanism, but it increases greatly with depth because of the increase in the pressure-work term in the exponential argument of the viscosity (see Sammis et al., 1977).

The rate of decrease in the thermal expansivity with depth is governed by the Anderson-Grueneisen parameter δ (e.g., Anderson, 1995). For olivine, δ was measured to be about 5 (Chopelas and Boehler, 1992), but for perovskite delta has recently been determined to be around 10 for the top 300 km of the lower mantle (Katsura et al., 2005). Such a high value would have profound effects in mantle dynamics, especially for slab penetration and the development of superplumes under the transition zone (Yuen et al., 1996).

The viscosity hill, depicted above, raises some interesting issues. Recent investigations on high-spin to low-spin transition of Fe++ in lower-mantle materials (Badro et al., 2004; Lin et al., 2005; Speziale et al., 2005; Tsuchiya et al., 2006) revealed the possibilities for electronic rearrangements of molecular bonding at pressures corresponding the depth of the viscosity hill, which is located around 1500 to 1800 km at depth (Mitrovica and Forte, 2004). Such a change in the electronic environment in that pressure range would have an unforeseen effect on the activation enthalpy of the lower-mantle assemblage, which would, in turn, invalidate the cherished idea of

a single activation energy and volume, commonly employed in rheological flow law used in modeling (e.g., Tackley, 1996).

We have employed the following numerical models for illustrating the dynamics of superplumes:

(1) Boussinesq, variable viscosity code, based on the finite-volume method and MPI parallelization, in both 2-D and 3-D Cartesian geometries (Trompert and Hansen, 1998).
(2) Anelastic compressible 3-D spherical-shell code, based on finite-differences and spherical harmonics (Monnereau and Yuen, 2002) and Open MP for multiple processors.
(3) Extended-Boussinesq variable viscosity code, based on finite-differences and and conjugate gradient methods in 2-D Cartesian geometry (Matyska and Yuen, 2005; Matyska and Yuen, 2006).
(4) Extended Boussinesq, variable viscosity code, based on finite-volume, pseudo-compressibility, multigrid and MPI parallelization (Kameyama et al., 2005; Kameyama, 2005).

Armed with this array of numerical tools, we can now proceed to explore various aspects of superplume dynamics.

3 RESULTS

3.1 2-D and 3-D Boussinesq models

We will begin with the simplest model taken from the Boussinesq convection equations with both constant thermal conductivity and thermal expansivity. A very wide, two-dimensional box with an aspect-ratio of 36 is taken. The viscosity law employed is temperature-and depth-dependent with the form of

$$\eta(\mathrm{T}, z) = z^n \exp(-100\mathrm{T}) \tag{5}$$

where T is dimensionless temperature and z is the dimensionless depth with $z = 0$ situating at the top. The parameter n controls the steepness of the depth-dependence of the viscosity and the location of the maximum of the viscosity profile, as a consequence of the interplay between the temperature-dependent viscosity and the depth portion of the viscosity. A larger n would move the maximum deeper down toward the core-mantle boundary. The maximum of the horizontally averaged viscosity profile in the lower mantle comes from the interaction between the increasing depth-dependence from the polynomial in z and the decreasing viscosity due to the temperature from the approach to the hot core-mantle boundary. The surface Rayleigh number of the simulations reported in this section is 10^7.

Figure 2 shows the dynamical influence of moving this viscosity hill deeper down. For $n = 2$ there are many upwellings, but with increasing n or greater degree of depth-dependence there is a diminishing number of plumes. Thus we see clearly the stabilizing influence of the depth-dependence of viscosity on mantle convection,

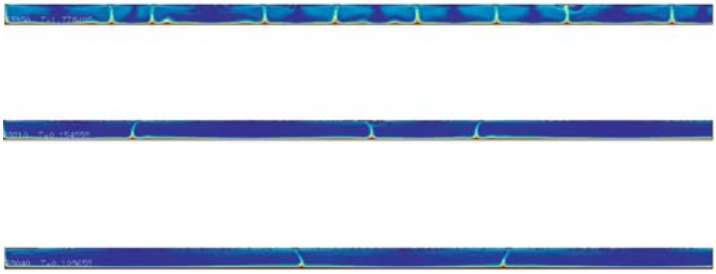


Figure 2. Temperature fields from two-dimensional Boussinesq convection with temperature- and depth-dependent viscosity. A constant thermal coefficient of expansion and constant thermal conductivity are used. Number of grid points used are 128 in the vertical direction and 2048 along the horizontal axis. An aspect-ratio of 36 is taken. We note that the index n in eqn. (5) goes from 2 to 5 to 10 for the three panels.

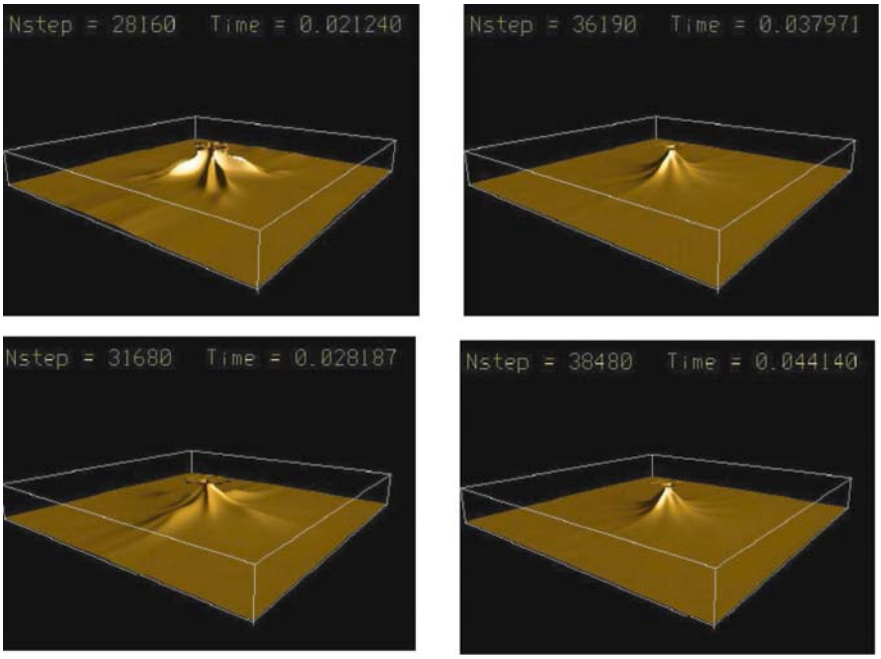


Figure 3. Isosurfaces of the temperature field of 3-D convection at four different times. The isosurface corresponds to T = 0.7, or about 2500 K. A time of 0.01 is around half the age of the Earth. The depth dependence of the viscosity has the form z^5 and the surface Rayleigh number is 10^7. The thermal coefficient of expansion decreases by 1/3 across the mantle in this Boussinesq model with an aspect-ratio of $4 \times 4 \times 1$. The number of grid points is 64 in the vertical and 128×128 on the horizontal plane.

which is a well-known result (Gurnis and Davies, 1986; Hansen et al., 1993). This example reveals that the particular style of plume dynamics and plume population can yield salient information about mantle viscosity stratification.

In plume dynamics it is important to verify the initial 2-D findings in 3-D geometry. Yuen et al., (1996) have already investigated the 3-D dynamical influence arising from

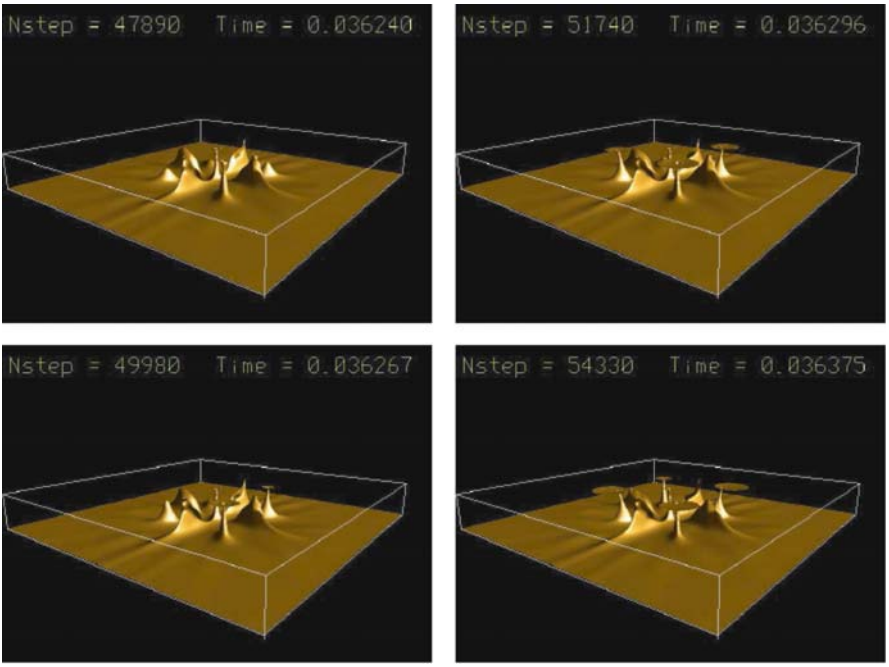


Figure 4. Isosurfaces of the temperature field of 3-D convection with temperature- and depth-dependent viscosity. The depth-dependence of viscosity is the same as in the previous figure but the temperature-dependence is given by exp(−100T). The composite viscosity is a product between the depth-dependent viscosity and the temperature-dependent portion. Otherwise, the rest of the information is the same as in Figure 3.

a viscosity profile, given analytically by a form with a dependence of a polynomial in z modulated by a Gaussian function whose center controls the location of the viscosity hill in the lower mantle. They found in a 3-D box with an aspect-ratio $6 \times 6 \times 1$ that there persisted one single very large plume for around fifty million years. In Figure 3 we verified this earlier result by integrating the solution much longer in time than previously. We note that there is a long evolution of this plume to the final equilibrium configuration shown in the bottom right panel.

It is well-known that temperature-dependent viscosity destabilizes the bottom boundary layer (Yuen and Peltier, 1980) and causes small-scale finite-amplitude instabilities (Christensen, 1984). In Figure 4 we show the long-time development of 3-D convection with the same depth-dependence in viscosity used in Figure 3 but now modulated with a temperature-dependent viscosity of the form exp(−100T).

As expected, we observe the development of small-scale instabilities with a tendency to cluster about a central location, as in a thermal attractor, a consequence

from plume-plume collisions (Vincent and Yuen, 1988). These plumes would march inward and then migrate outward again in a quasi-periodic fashion. Clustering of small-scale plumes in the deep mantle has been invoked by Schubert et al., (2004) as an alternative explanation for superplume province under the central Pacific on the basis of tomographic imaging. We are quite heartened by the recent result by Yoshida and Kageyama (2006), who also demonstrated quite convincingly that for 3-D spherical convection the combination of temperature- and depth-dependent viscosity also preserves the same long-wavelength circulation found here in Cartesian geometry with a similar type of hybrid temperature- and depth-dependent rheology.

3.2 3-D Anelastic compressible spherical-shell model

As in Monnereau and Yuen (2002), we have employed the PREM model (Dziewonski and Anderson, 1981) for the reference density profile and the bulk modulus, which is needed for handling the compressibility of mantle material in long term deformation. The depth-profiles for the density, bulk modulus and the thermal expansivity are exponential functions that fit PREM and are shown in Monnereau and Yuen (2002). The thermal expansivity α is obtained by assuming a constant value of the Grueneisen parameter of unity and a usual value of the specific heat at constant pressure of 1200 J kg^{-1} K^{-1}. The thermal expansivity decreases across the lower mantle by a factor of 2. It decreases a factor of 4 across the mantle. We have not considered the effects of variable thermal conductivity with temperature and pressure (Dubuffet et al., 1999).

The mantle convection models studied here are both heated below, and also internally heated by radiogenic elements, which do not decay with time. There are two Rayleigh numbers, the basal heating Rayleigh number Ra and the internal-heating Rayleigh number, Ra_i. The internal heating has been set to a common value of 25 TW of contributed surface heat released, which corresponds to about 1.5 times the chondritic heating contribution. In Monnereau and Yuen (2002) the internal heating was varied between 0 and 60 TW.

It is well known from past work (e.g., Zhang and Yuen, 1995) that plume dynamics in 3-D spherical convection in basally heated configuration are very much affected by the depth variations of mantle viscosity. The effects of including internal heating, mantle compressibility and viscosity stratification on enhancing the vigor of plume growth have been shown by Zhang and Yuen (1996) and also by Bunge et al. (1996). We have employed eight different viscosity profiles for the purpose of understanding the influence of the deep mantle viscosity stratification on the style of plumes. We have considered profiles ranging from constant viscosity to classical two-layered viscosity models (e.g., Ricard et al., 1984), and extending to more complex viscosity profiles inferred from both geoid anomalies and post-glacial rebound analysis (Mitrovica and Forte, 2004). Walzer et al. (2004) have studied the influence of a family of depth-dependent viscosity profiles in 3-D anelastic compressible convection but did not focus on the development of thick upwellings in the lower mantle.

We have parameterized the viscosity models with a series of layers instead of using analytic functions for describing the sharp variations of the viscosity peaking the mid lower-mantle, as in Zhang and Yuen (1996) or in Yuen et al. (1996). The first five models have been designed to highlight the basic effects of a viscosity hill in the lower mantle. Model 1 is a constant viscosity model. Model 2 is one introduced by Ricard et al. (1984) and Hager and Richards (1989) and has a viscosity increase of 30 across the 660 km phase change. Model 3 is Model 2 including a low viscosity zone (LVZ) of 200 km thick above the CMB. Model 4 and 5 are similar to Model 2 and 3 respectively, but with a viscosity contrast of 300 instead of 30. The three following models have a more complex viscosity structure, taken from recent geoid/postglacial rebound/tomographic analysis. Model 6 (FM) comes from Forte and Mitrovica (2001) in which there are tow prominent viscosity peaks in the lower mantle at a depth of around 900 km and 1800 km. Model 7 (RW) is the viscosity model derived by Ricard and Wuming (1991). The last viscosity model (MF) derives from the recent viscosity profile (Mitrovica and Forte, 2004) based on both geoid anomalies and glacial isostatic readjustment. These viscosity profiles are shown below in Figure 5.

Figure 6 presents the thermal anomaly fields of 3-D spherical convection, i.e., the deviation from the horizontally averaged temperature, of the first 5 cases of the viscosity profiles displayed in Figure 5.

- Case 1: in this constant viscosity case, mantle convection is dominated by downwellings, which is expected with a strong internal heating (77%). The downwellings exhibit a linear shape at the surface, and adopt a cylindrical structure below triple junctions. Only these cylindrical downwellings cross the phase change at 660 km discontinuity. These features fluctuate and do not remain at one place. The hot plumes are less vigorous and remain restricted to the lower mantle.
- Case 2: with the introduction of a stepwise viscosity increase of 30 across the 660 km phase boundary, three large plumes develop and now drive the circulation. Shorter scales than in the previous case feature the downwellings. Their structure remains perceptible in the lower mantle, indicating a decrease of the strength of the phase change barrier. These structures are very close to the one described by Dubuffet et al. (2000) in 3-D Cartesian with the same kind of viscosity profile and 80% of internal heating. Here, it amounts 73% of the total heat flux. It is worth noting that large plumes can develop with intense internal heating and are not only the consequence of pure basal heating. The viscosity increase with depth is well known to cause a cascade to longer wavelengths in the thermal spectrum, but it is much less known to promote large stable hot plumes even when internal heating is dominant. This could be understood, if we point out that another major effect of the viscosity increase with depth is to reduce the ambient temperature and thus to enhance the temperature contrast across the bottom thermal boundary layer. This naturally results from the disequilibrium between the top and the bottom boundary layers introduced by the viscosity contrast. As a matter of fact, the averaged temperature is here 500 K lower than in the previous constant viscosity case for a temperature contrast twice larger.

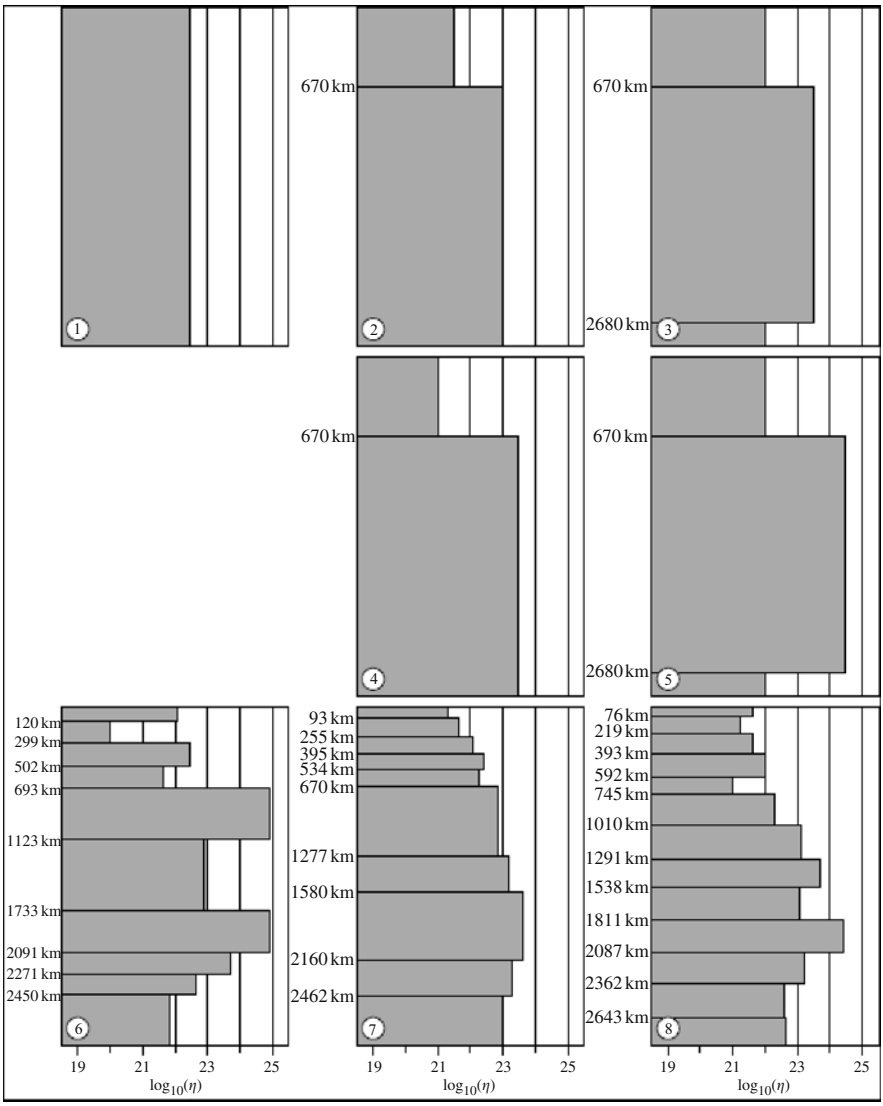


Figure 5. Viscosity profiles used in the 3-D spherical-shell convection model. The first five will be used in Figure 6 and the last three in Figure 7.

- Case 3: we add a 200 km thick low viscosity zone at the CMB, which can be expected, as the viscosity strongly depends on temperature. The viscosities at the CMB and in the upper mantle are the same; so that the disequilibrium between boundary layers previously invoked is strongly reduced, but not entirely because

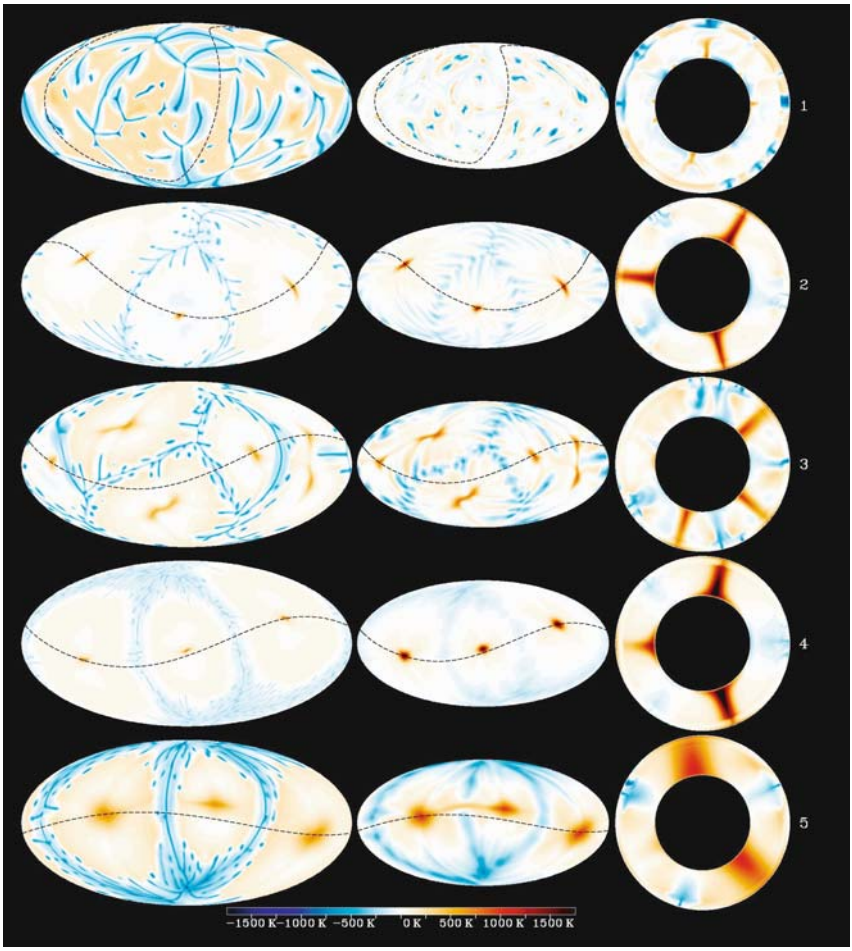


Figure 6. Thermal anomalies of 3-D convection in spherical shell. The horizontal cross-sections associated with the left column are taken at a depth of 500 km, the images of the central column comes from a depth of 1500 km in the mid lower-mantle and the right column contains a global vertical cross section of the entire mantle, whose great circle path is shown in both the upper- and lower-mantle horizontal projections in the left and central columns respectively. Blue color indicates cold downwellings, while the brown color represents hot upwellings. The temperature of the CMB is 3200 K.

of the spherical geometry that produces a similar effect (e.g., Jarvis, 1993). From this point of view, case 1 and 3 may appear analogous. In spite of this similarity, six large plumes develop and the cold structures at the surface keep the features exhibited in case 2. It seems that the high viscosity region in the middle of the mantle plays the role of low-pass filter for the dynamics. This will be highlighted by comparing the two following cases, 4 and 5, where the viscosity profiles exhibit

the same features as in cases 2 and 3 respectively, except in the amplitude of the viscosity contrast.

- Case 4: the viscosity contrast has been raised up to 300. The dynamics develops a structure very similar to case 2, but with shorter wavelength cold currents at the surface. This probably results from the choice of a lower value for the reference viscosity, made in order to keep comparable heat fluxes from one case to another. The main difference is that the hot plumes are now roughly twice thicker than in case 2. We can discern the strong narrowing of these plumes upon crossing the viscosity jump.
- Case 5: in contrast to case 3, the addition of the low viscosity zone at the CMB, does not change the number of plumes. Furthermore, their broad shape is reinforced. They appear like thick vertical cylinders standing atop the CMB.

A viscosity increase with depth is now well known to promote large plumes with long-wavelength circulation in the lower mantle (Hansen et al., 1993), notably through the disequilibrium between boundary layers it introduces. However, if a general depth dependence of the mantle viscosity is expected, the large temperature of the bottom boundary layer should reduce the viscosity and attenuate this effect. We see here that the viscosity stratification effect acts more than a perturbation to the boundary layers and that the presence of a viscosity hill in the middle of the mantle plays the important role of a low pass filter, preventing the onset of short wavelength instabilities at the expense of very broad structures.

Figure 7 displays the temperature anomaly fields of the three remaining cases that correspond to more complex viscosity profiles. At first sight, the expression of mantle convection strongly differs from one case to the other, except in the fact that hot plumes are well established in the lower mantle. There is only one in the case 6, three in case 7, and two in the last case that are distributed along a hot line drawing a great circle at the core surface. The single plume mode that characterizes case 6 has only been found under peculiar conditions: with a small core radius to mantle thickness ratio (Schubert et al., 1990, Moser et al., 1997), or with an endothermic phase change slightly above the CMB (Breuer et al., 1998; Harder and Christensen, 1996). Both situations have been invoked to account for the formation of the Tharsis highlands. These conditions act also in previously described ways: either as a strong imbalance between the local Rayleigh number of boundary layers for the former, or as a low pass filter for the latter. In case 6, the second effect should prevail, enhanced by the presence in the viscosity profile of two maxima peaking three orders of magnitude above the values at the top and the bottom. It is worth noting that, in this case, both upwellings and downwellings are filtered in the same way: the single hot plume being associated with a single cold plume.

More than just the dominance of large hot plumes in the lower mantle, the striking feature rising from the comparison of cases 6, 7 and 8, is the remarkable sensitivity of the upper mantle dynamics to the viscosity profile structure. In case 6, both the hot and cold plumes can cross the whole mantle. The thermal field does not reveal any layering of the dynamics that would be associated with the endothermic phase

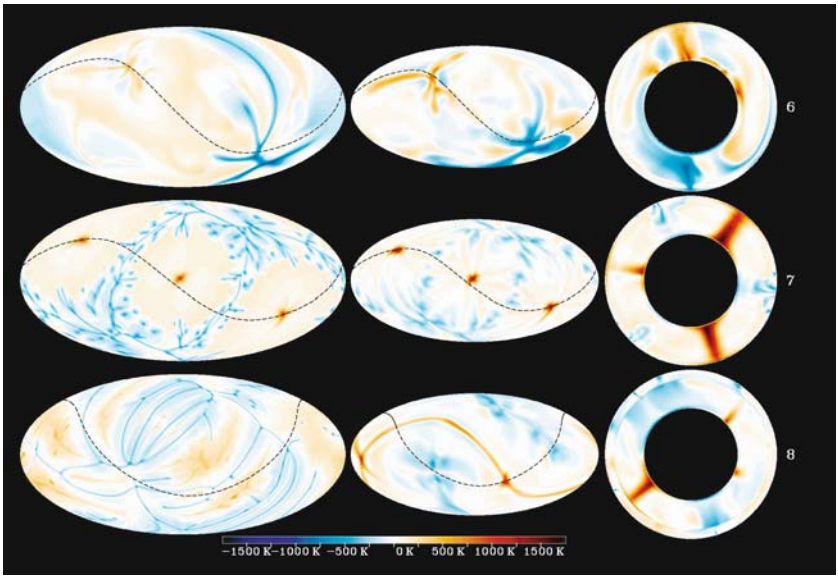


Figure 7. Temperature anomalies of the last three viscosity cases shown in Figure 5. Otherwise, the same information is provided as in Figure 6.

change. In case 7, there is no longer any stratification, but the downwelling structure is quite different from the upwelling one. The asymmetry is close to the one observed in cases 2–5, what would be expected since the viscosity profile proposed by Ricard and Wuming (1991) is also close to the schematic ones introduced in cases 2–5. Case 8 reveals a completely different situation. Here, mantle convection splits into two parts. This is an expected and well-known effect of the endothermic phase change (e.g., Christensen and Yuen, 1985), but that does not necessarily occur, particularly when mantle properties are depth-dependent (Bunge et al., 1996; Monnereau and Rabinowicz, 1996). As a matter of fact, no layering is observed in the previous cases when the viscosity increases with depth. Furthermore, the decoupling, that takes place here, does not behave as the famous intermittent layering highlighted first by Machetel and Weber (1991), where a recurrent rupture of the quite impermeable barrier induced by the phase change precipitates an intense and rapid mass exchange between the upper and lower mantle. Such catastrophic events are more related to the 2-D approximation of numerical experiments, where they have only been observed. Conversely, the mass flux across the phase change is here roughly constant with time, but varies strongly from place to place; the layering is not discontinuous in time but in space. For instance, the surface expression of the huge plumes established in the lower mantle is not a single hot spot as in case 7, but a cluster of small plumes that develop in the area where the lower mantle plume impinges the phase change. It is also worth noting the presence of rolls between two clusters of plumes, oriented perpendicularly

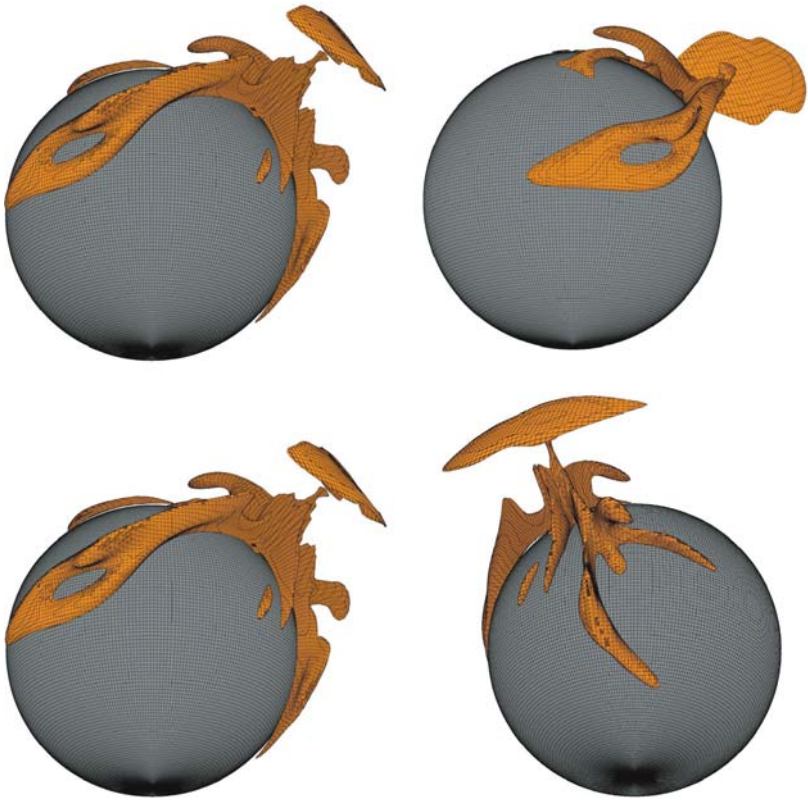


Figure 8. Isosurfaces of hot temperature showing the single plume with a very long ridge-like feature similar to the Great Chinese Wall. The isosurface corresponds to T = 0.7, or about 2700 K.

to the underneath hot line. Such a decoupling between the upper and lower mantle, searched for a long time, mainly results from a low viscosity zone located under the phase change. The role of such a low viscosity zone has been discovered by Kido and Cadek (1997) and well described in a dynamical sense by Cserepes and Yuen (1997). We see in the upper-mantle of case 8 the presence of Richter rolls (Richter and Parsons, 1975) in the left-most panel. These secondary cellular motions are caused by the low-viscosity zone underneath the transition zone. In Figure 8 we take a more detailed look at the ridge-like structures developed in case 8, in which a single plume is found (see Fig. 7).

One striking character of these isosurfaces is that these thermal convective results in spherical geometry appear very similar to ridge-like features obtained in thermal-chemical convection in 3-D Cartesian geometry (e.g., Tackley, 2002). They are similar to the lower-mantle mountain-like feature, reminiscent of the Great Wall of China, which was inferred by Ni and Helmberger (2003), using forward-modelling techniques. See also article by Maruyama et al., in this issue. The factor which

may produce this distinct signature is the steep viscosity stratification in the deep mantle, imposed by the viscosity profile 8, shown in Figure 5. Thus there is a trade-off between thermal-chemical convection and the depth-dependence of viscosity in the production of sharp ridge-like features in lower mantle thermal convection. In laboratory experiments only thermal-chemical aspects can be investigated, while numerical simulations are able to shed light in fluid dynamical situations with depth-dependent properties. The different factors determining the ridge-like features need to be studied in 3-D spherical geometry. Here the influence of the post-perovskite phase transition should also be accounted for, as well as chemical heterogeneities and equations of state of deep mantle components (Tan and Gurnis, 2005). We note that the recent calculations by Yoshida and Kageyama (2006) in 3-D spherical shell show quite convincingly that strong temperature-dependent viscosity cannot override the long-wavelength circulation enforced by depth-dependent viscosity in the lower mantle.

3.3 2-D Extended-Boussinesq Cartesian model with variable viscosity and phase transitions

Up to now, we have not included the effects of phase transitions in both the upper- and lower-mantle, which can surely influence the development of superplumes. The two phase transitions considered are the endothermic spinel to perovskite transition separating the upper- and lower-mantle and the exothermic post-perovskite transition (Murakami et al., 2004; Oganov and Ono, 2004; Tsuchiya et al., 2004) in the deep mantle. The phase transitions have been implemented by using the formulation of an effective thermal expansivity (Christensen and Yuen, 1985). The density changes of the two phase transitions are respectively 8 and 1.5% and the Clapeyron slopes are -3 MPa/K and $+9$ MPa/K. Besides the phase transitions, we will also incorporate a depth-dependent thermal expansivity, which drops by a factor of 2 in the upper mantle but decreases sharply in the shallow portion of the lower mantle right below the transition zone (Katsura et al., 2005) with a total drop of a factor of around 11 across the lower mantle, because of the large value of the Anderson-Grüneisen parameter for perovskite in the shallow part of the lower-mantle (Katsura et al., 2005; R. M. Wentzcovitch, private communication, 2006). We employ a temperature- and depth-dependent viscosity, where the depth-dependent portion is prescribed by a product between a linear function in z and a Gaussian in z which peaks in the middle of the lower mantle and a temperature-dependent portion, which varies exponentially in T. The viscosity hill in the lower mantle at a depth of around 1700 km is about a factor of 150 greater than the viscosity in the upper mantle, while the variations of the temperature-dependent viscosity are around 1000. The full formulation of the viscosity law can be found in Matyska and Yuen (2006).

We have also employed a radiative thermal conductivity $k(\mathrm{T})$ of the canonical form:

$$k(\mathrm{T}) = f \cdot (\mathrm{T} + \mathrm{T}_0)^3 , \tag{6}$$

where f is an enhancement factor, here taken to be 10, and T_0 is the surface temperature, here $T_0 = 0.08$. We have considered three kinds of conductivity model (1) constant thermal conductivity in the entire mantle (2) radiative thermal conductivity just in the D″ layer and constant thermal conductivity in the rest of the mantle (3) radiative thermal conductivity in the entire mantle. We will consider these three cases for thermal conductivity in this section, while all the other thermodynamical and rheological parameters remain the same.

Relatively large aspect-ratio cells are developed but with large asymmetries in the behavior, primarily due to the hotter interior of the right cell. The style of plume dynamics is very much different in the two regions. In the left cell we observe many traveling-wave instabilities, while a large cluster of upwellings is developed in the right cell. Secondary upwellings (see also Yoshida and Ogawa, 2004) are emerging from the spinel to perovskite transition in both right and left cells. The bottom boundary layer is highly unstable due to the exothermic post-perovskite phase transition (Nakagawa and Tackley, 2004a; Matyska and Yuen, 2005).

Next we show the case in which the thermal conductivity is constant everywhere except for a thin post-perovskite layer, in which the thermal conductivity is now radiative.

Comparing Figures 9 and 10, we see the dramatic difference in convection caused by just a thin layer of radiative thermal conductivity. The imposition of a thin radiative layer exerts unexpectedly a substantial influence on the style of mantle convection, because of the ability of radiative transfer to bring up very efficiently an enormous amount of heat from the hot outer core at a temperature of 3880 K. The upwellings developed are very broad in character and heats up the lower mantle. There is a pool of super-heated material (blue color) lodged right under the transition zone in the right cell.

We compare the previous case with a model in which radiative thermal conductivity is prevalent throughout the entire mantle (Fig. 11).

The global presence of radiative thermal conductivity induces thinner upwellings in both cells, because of the better developed bottom boundary layer and stronger thermal buoyancy inside the plumes, which lead to higher velocities and greater contrast between the thinner superplume and the adjacent lower mantle. Moreover, there is a greater mass flux of lower-mantle material penetrating the 670 km discontinuity, which produces bigger upper-mantle plumes. We observe plumes branching off the transition zone, as rendered artistically earlier by Maruyama (1994). Thus the spatial distribution of radiative thermal conductivity can significantly affect the style of superplumes. This has a similar effect, as the spatial distribution of mantle viscosity. The main purpose of this sub-section is to emphasize the importance of variable thermal conductivity on modulating upwellings in the lower mantle. Thermal conductivity can also be enhanced in the D″ layer for other reasons than radiative transfer. For instance, some infiltration of Fe melt (Petford et al., 2005; Kanda and Stevenson, 2006) can also greatly increase the local thermal conductivity of the D″ layer (Manga and Jeanloz, 1996) and also the putative presence of FeS can also increase the local thermal conductivity (Hofmeister and Criss, 2005).

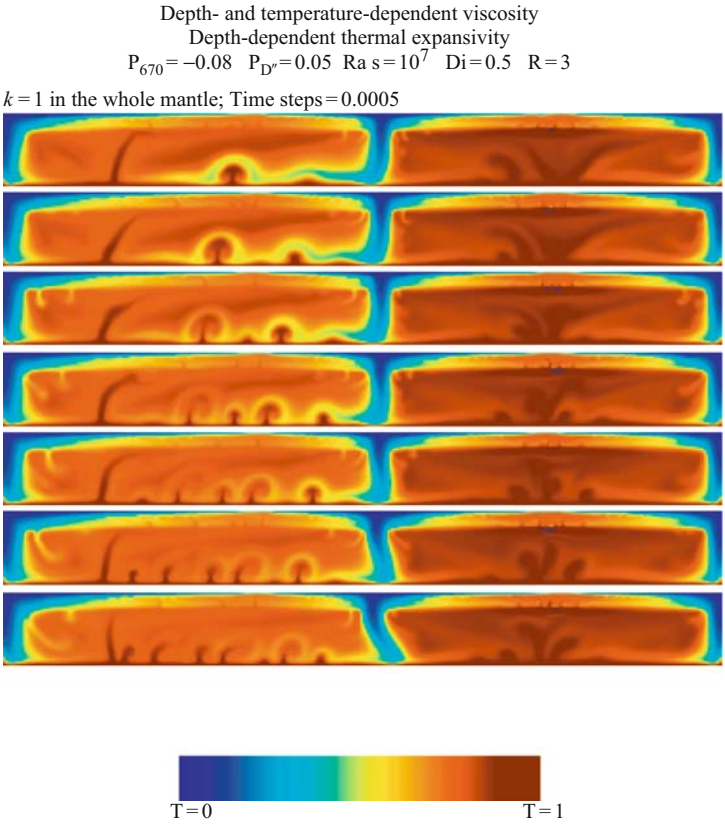


Figure 9. Temperature fields of 2-D extended-Boussinesq convection with constant thermal conductivity, temperature- and depth-dependent viscosity, depth-dependent thermal expansivity, two phase transitions in the upper- and lower- mantle. An aspect-ratio 10 has been assumed. The surface dissipation number is 0.5 and the surface Rayleigh number is 10^7. There is a small amount of internal heating, about 25% of the chondritic value with R = 3. We have used a periodic color scale, i.e., dark blue region below the 660 km boundary shows the places, where the dimensionless temperatures are slightly greater than 1, i.e., greater than the temperature at the core-mantle boundary!

3.4 Three-dimensional extended-Boussinesq convection in Cartesian geometry with variable properties and phase transitions

Now we turn our attention to the 3-D effects in Cartesian geometry in a box having an aspect-ratio of $6 \times 6 \times 1$. We use variable properties in thermal conductivity, viscosity and depth-dependent thermal expansivity along with the two major phase transitions in the upper- and lower-mantles. This particular numerical model, which employs the primitive variable formulation (velocity, pressure and temperature), has already been described in great technical details in Kameyama et al. (2005) and Kameyama

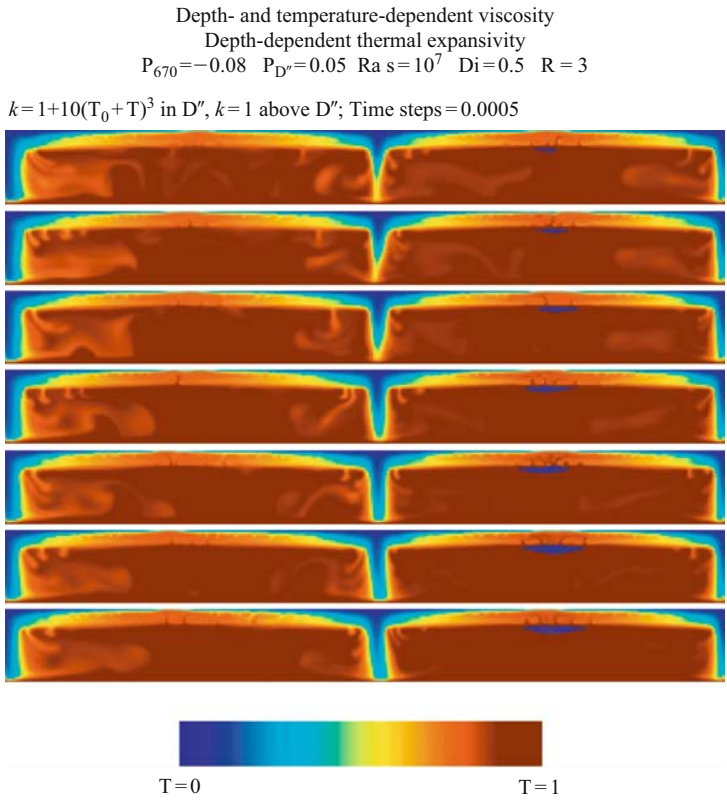


Figure 10. Two-dimensional temperature field from extended-Boussinesq convection with a thin layer (180 km) of radiative thermal conductivity at the bottom. Other parameters are the same as in Figure 9. We have used a periodic color scale, i.e., dark blue region below the 660 km boundary shows the places, where the dimensionless temperatures are slightly greater than 1, i.e., greater than the temperature at the core-mantle boundary!

(2005). The relationship for temperature- and depth-dependent viscosity is similar to the one employed by Matyska and Yuen (2006). This means that the viscosity variation is about a factor of 100 for temperature and 155 for the depth. We have used a temperature-dependent thermal conductivity of the radiative type, very similar to the form given in Matyska and Yuen (2006). The thermal coefficient of expansion is of the same form given in Matyska and Yuen (2005) and decreases by a factor of 8/27 across the mantle. There is a small amount of internal heating with a strength, which is one quarter that of chondritic abundance. The temperature of the CMB is taken to be 3888 K.

For describing the dynamics of the phase transitions, we have employed the formulation of an effective thermal coefficient of expansion (Christensen and Yuen, 1985).

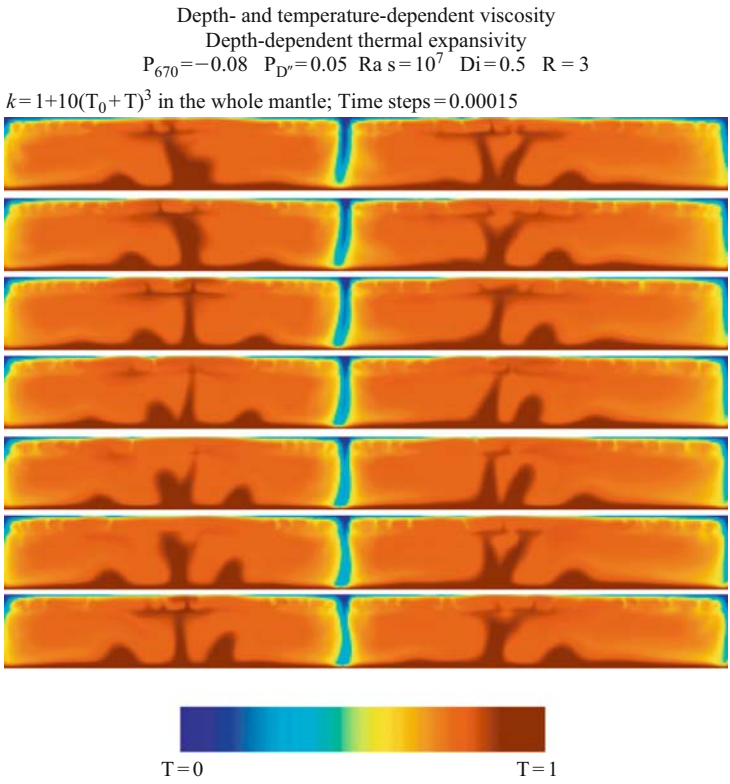


Figure 11. Two-dimensional temperature field from extended-Boussinesq convection with radiative thermal conductivity present throughout the mantle. Other parameters are the same as in Figure 9.

The computational domain consists of 256 × 256 × 64 grid points based on a finite-volume scheme (Kameyama, 2005). This run required over 200,000 time-steps and was carried out on the Earth Simulator computer.

In Figure 12 we show four snapshots of the isosurface of hot upwellings with T = 0.7, covering an interval of time of around 2 Byrs.

The upwellings are unlike the classical type of plumes one would find in laboratory thermal convection or numerical simulations with a simple temperature-dependent rheology (Whitehead and Parsons, 1976; Jellinek et al., 1999; Zhong et al., 2000) and instead they appear closer to those found in thermal-chemical convection (Davaille et al., 2005). These upwellings are characterized by ridge-like structures, similar to the results found in Figure 8 for depth-dependent viscosity in 3-D spherical geometry. The structures develop a dynamical time-dependent pattern, characteristic of being in the thermal-attractor regime (Vincent and Yuen, 1988), with the plumes first marching toward the center and then moving back out. Such a scenario can be likened

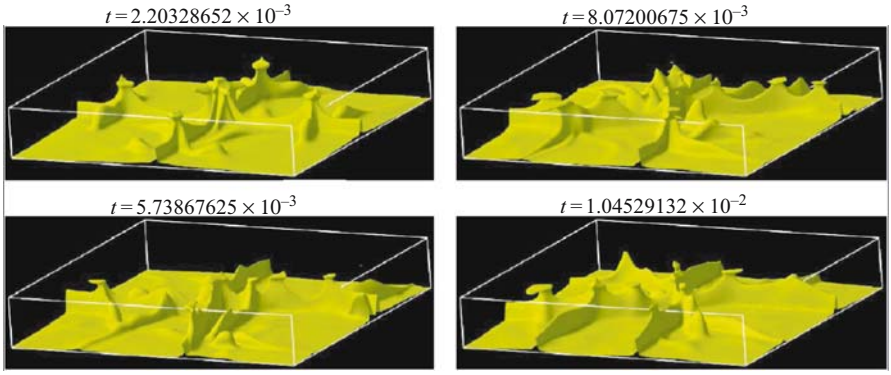


Figure 12. Snapshots of isosurfaces of hot temperature fields in convection with variable properties and two major phase transitions. The temperature of the isosurface corresponds to 2717 K. A dimensionless time of 0.001 represents around 288 Myrs.

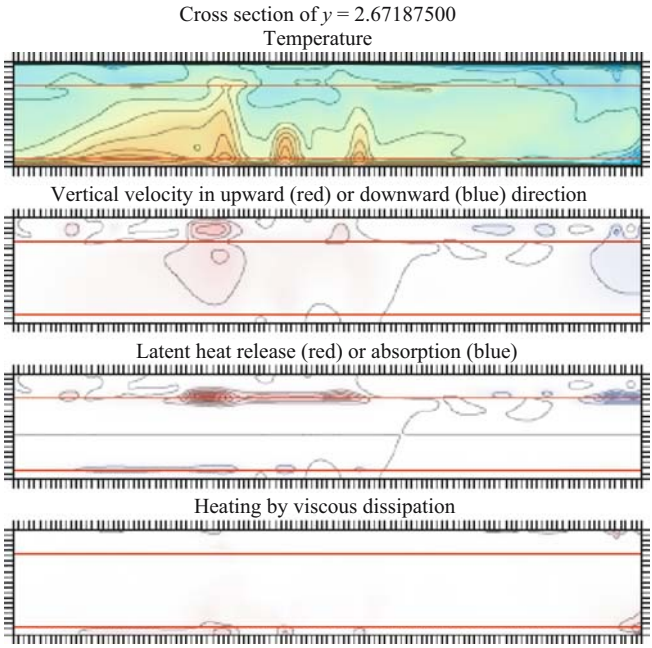


Figure 13. Two-dimensional cross-sections of the temperature, vertical velocity, latent-heat released and viscous dissipation. These fields are taken from the 3-D fields associated with the last time instant in Figure 12. The vertical velocity, latent-heat released and viscous dissipation have been normalized respectively to 57500, 9090 and 155, the maxima of these fields, given in dimensionless units. This is a vertical cross section taken at the horizontal coordinate $y = 2.67$.

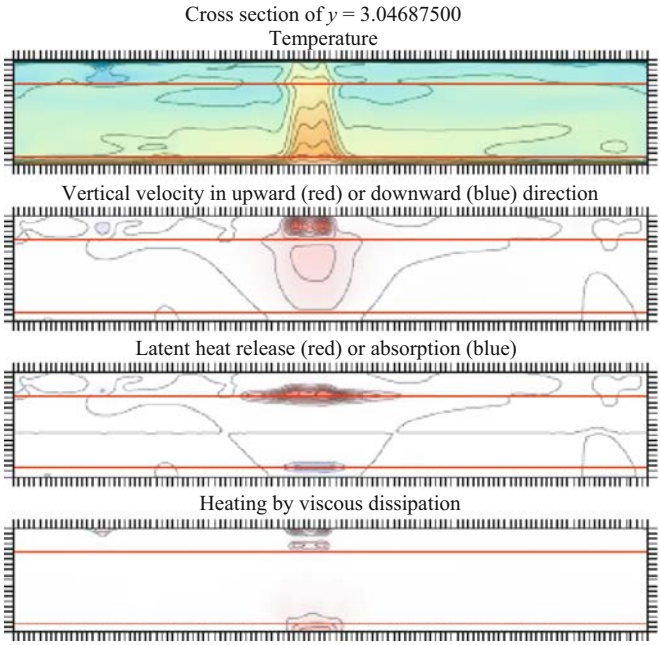


Figure 14. Two-dimensional map of the temperature, vertical velocity, latent-heat budget and viscous dissipation. This is a vertical cross-section taken at $y = 3.05$. Otherwise, the rest is the same as in Figure 13.

to the plume cluster model, as envisioned in Schubert et al. (2004). The proximity of the post-perovskite phase transition to the core-mantle boundary strongly promotes the growth of boundary-layer instabilities with a rich spectral content. The developed upwellings are then moderated by the radiative thermal conductivity (Matyska and Yuen, 2005). Clearly more work is needed in understanding the growth of plume-like structures under these complex physical conditions in the deep mantle.

From the last time instant, we take three 2-D cross-sections in order to understand better the thermo-mechanical structures associated with this type of 3-D thermal convection. These cross sections are taken very close to the intersection of the two ridges near the center of the box (Figs. 13 and 14).

In this perspective we can see from the vertical velocity contours that layered convection prevails with small rolls in the upper mantle. There is a broad-scale upwelling with several small-scale instabilities at the bottom. There is some small-scale shear-heating in the D″ layer and a large-amount of latent-heat released at the base of the transition zone (Steinbach and Yuen, 1994). The fastest plumes are found in the upper mantle.

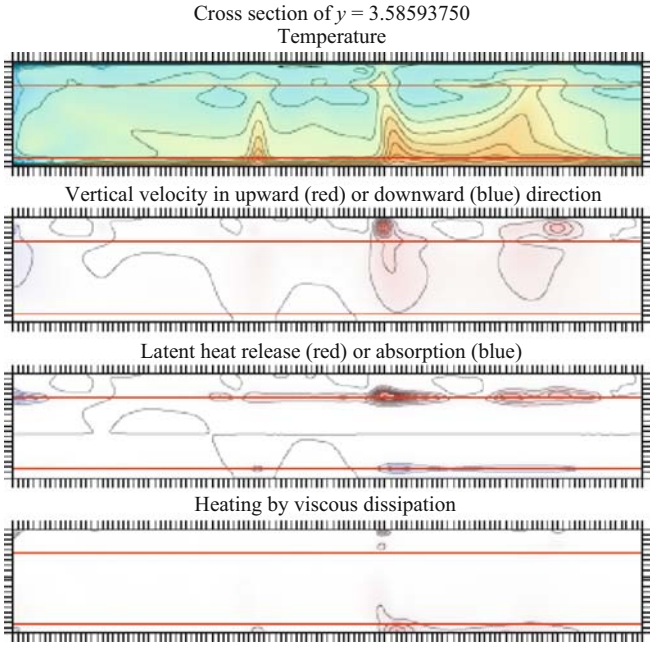


Figure 15. Two-dimensional map of the temperature, vertical velocity, latent-heat budget and viscous heating. This is a vertical cross-section taken at $y = 3.59$. Otherwise, the rest is the same as in Figure 13.

Close to the interaction of the two ridges, we can observe a relatively broad upwelling having a width exceeding 800 km. There is a fast upwelling in the upper mantle associated with this thick root. Large amounts of latent heat released takes place in the transition zone. There is also some shear heating developed in this upwelling. The nature of layered convection with multiple-scales in the flow field is clearly displayed by the vertical velocity field.

The last cross section (Fig. 15) shows again the multi-scale nature of this type of thermal convection with partial layering. There is a large asymmetry in the velocities of the flow field between the upper and lower mantle. We see that small-scale convection takes place in the upper-mantle above the rising superplume in the lower mantle. This shows the need to incorporate as many physical mechanisms as possible in order to account for the diversity of scales in mantle plume dynamics (e.g., Courtillot et al., 2003; Yoshida and Ogawa, 2004).

4 CONCLUSION

In this chapter we have gone over the primary mechanisms in the generation of lower-mantle plumes by thermal convection. We have identified several key ingredients, which will promote the development of superplumes. They include (1) the style of

viscosity increase in the lower mantle, especially that due to the viscosity maximum in the lower mantle at a depth of around 1800 km (e.g., Forte and Mitrovica, 2001) (2) the decrease in the coefficient of thermal expansion (3) the increase of thermal conductivity from radiative contribution in the deep portion of the lower mantle. We may also consider other potential contribution, such as the influence from grain-size dependent rheology (Korenaga, 2005), which has been suggested as a possible mechanism for generating superplumes in the D″ layer, but this hypothesis remains to be verified by either a decisive laboratory experiment or accurate numerical simulations.

The nature of the thermal boundary layer near the CMB would change with time because of the onset of the post-perovskite phase transition in the hot deep mantle with a cooling core, as first suggested by Oganov and Ono (2004). The exothermic phase transition would alter the nature of upward heat transfer by the growth of superplumes, because of the presence of either radiative thermal conductivity and/or grain-size changes from the post-perovskite phase transition. Thus superplumes can transport a great deal of heat from the CMB into the upper mantle, much more than traditional models without the post-perovskite phase transition (e.g., Mittelstädt and Tackley, 2006).

Finally, we should explore next the alternative route of superplumes having a predominant thermal-chemical origin. Up to now, all of thermal-chemical models (e.g., Mc Namara and Zhong, 2004; Nakagawa and Tackley, 2005) have employed simple models in lower-mantle rheology, thermal expansivity, compositional stratification and thermal conductivity. In the future it is necessary to incorporate more realistic multicomponent equations of state (Tan and Gurnis, 2005) and phase diagrams in both the upper- and lower mantles e.g., the majorite transition at high temperatures by Hirose (2002) in order to make a better assessment as to the relative efficacy in producing superplume structures between the thermal and thermal-chemical end-members in a compressible mantle convection.

ACKNOWLEDGEMENTS

We thank stimulating discussions with Cesar da Silva, Renata Wentzcovitch, Anne Hofmeister, and Shigenori Maruyama, which have improved greatly this manuscript. We are grateful to Marina and Katya Shukh and Ying-chun Liu for their skillful help in preparing this chapter. This research has been supported by the Math-Geo, CSEDI and ITR programs of the U.S. National Science Foundation (DAY), the Stagnant Slab Project, Scientific Research in Priority Areas of Ministry of Education, Culture, Sports and Technology of Japan (MK), the Deutsche Forschungs Gemeinschaft (UH), and the Czech Science Foundation grant 205/03/0778 (CM). The calculations presented in this paper were carried out in Earth Simulator at Japan Agency for Marine–Earth Science and Technology, French CNES, Minnesota Supercomputer Institute, Prague and Univ. of Münster in Germany.

REFERENCES

Anderson, O.L. (1995) Equations of State of Solids for Geophysics and Ceramic Science, 405pp, Cambridge Univ. Press.

Badro, J., G. Fiquet, F. Guyot, J.-P. Rueff, V.V. Struzhkin, G. Vanko, and G. Monaco (2003) Iron partitioning in Earth's mantle: Toward a deep lower mantle discontinuity. *Science*, 300, 789–791.

Breuer, D., D.A. Yuen, T. Spohn, and S. Zhang (1998) Three-dimensional models of Martian convection with phase transitions. *Geophys. Res. Lett.*, 25(3), 229–232.

Bunge, H.-P., M.A. Richards, and J.R. Baumgardner (1996) Effect of depth-dependent viscosity on the planform of mantle convection. *Nature*, 379, 436–438.

Chopelas, A., and R. Boehler (1992) Thermal expansivity of the lower mantle. *Geophys. Res. Lett.*, 19, 1983–1986.

Christensen, U.R. (1984) Instability of a hot boundary layer and initiation of thermo-chemical plumes. *Annal. Geophys.*, 2, 311–320.

Christensen, U.R., and D.A. Yuen (1985) Layered convection induced by phase transitions. *J. Geophys. Res.*, 90, 10291–10300.

Courtillot, V., A. Davaille, J. Besse, and J. Stock (2003) Three distinct types of hotspots in the Earth's mantle. *Earth and Planet Sci. Lett.*, 205, 295–308.

Cserepes, L., and D.A. Yuen (1997) Dynamical consequences of mid-mantle viscosity stratification on mantle flows with an endothermic phase transition. *Geophys. Res. Lett.*, 24, 181–184.

Davaille, A. (1999) Simultaneous generation of hotspots and superswells by convection in a heterogeneous planetary mantle. *Nature*, 402, 756–760.

Davaille, A., E. Stutzmann, G. Silveira, J. Besse, and V. Courtillot (2005) Convective patterns under the Indo-Atlantic. *Earth Planet. Sci. Lett.*, 239, 233–252.

Davies, J.H. (2005) Steady plumes produced by downwellings in Earth-like vigor spherical whole mantle convection models. *Geochem. Geophys. Geosys.*, 6(12), Q12001, doi:10.1029/2005GC001042.

Dubuffet, F., D.A. Yuen, and M. Rabinowicz (1999) Effects of a realistic mantle thermal conductivity on the patterns of 3-D convection. *Earth Planet. Sci. Lett.*, 171, 401–409.

Dubuffet, F., and D.A. Yuen (2000) A thick pipe-like heat-transfer mechanism in the mantle: Nonlinear coupling between 3-D convection and variable thermal conductivity. *Geophys. Res. Lett.*, 27(1), 17–20.

Dubuffet, F., M. Rabinowicz, and M. Monnereau (2000) Multiple-scales in mantle convection. *Earth Planet. Sci. Lett.*, 178, 351–366.

Dubuffet, F., D.A. Yuen, and E.S.G. Rainey (2002) Controlling thermal chaos in the mantle by positive feedback from radiative thermal conductivity. *Nonlinear Proc. Geophys.*, 9, 311–323.

Dziewonski, A.M., and D.L. Anderson (1981) Preliminary reference earth model (PREM). *Phys. Earth Planet. Inter.*, 25, 297–356.

Dziewonski, A.M. (1984) Mapping the lower mantle: Determination of lateral heterogeneities in P velocity up to degree and order 6. *J. Geophys. Res.*, 89, 5929–5952.

Forte, A.M., and J.X. Mitrovica (2001) Deep-mantle high-viscosity flow and thermochemical structure inferred from seismic and geodynamic data. *Nature*, 410, 1049–1056.

Grand, S.P., R.D. van der Hilst, and S. Widiyantoro (1997) Global seismic tomography: A snapshot of convection in the Earth. *GSA Today*, 7(4), 1–7.

Gurnis, M., and G.F. Davies (1986) Numerical study of high Rayleigh number convection in a medium with depth-dependent viscosity. *Geophys. J.R. Astr. Soc.*, 85, 523–541.

Hager, B.H., and M.A. Richards (1989) Long-wavelength variations in Earth's geoid: Physical models and dynamical implications. *Phil. Trans. R. Soc. Lond. A*, 328, 309–327.

Haken, H. (1983) Advanced Synergetics, 356pp, Springer Verlag, Berlin.

Hansen, U., and D.A. Yuen (1989) Dynamical influences from thermal-chemical instabilities at the core-mantle boundary. *Geophys. Res. Lett.*, 16, 629–632.

Hansen, U., D.A. Yuen, S.E. Kroening, and T.B. Larsen (1993) Dynamical consequences of depth-dependent thermal expansivity and viscosity on mantle circulations and thermal structure. *Phys. Earth Planet. Inter.*, 77, 205–223.

Harder, H., and U.R. Christensen (1996) A one-plume model of Martian mantle convection. *Nature*, 380, 507–509.

Hirose, K. (2002) Phase transitions in pyrolitic mantle around 670-km depth: Implications for upwellings of plumes from lower mantle. *J. Geophys. Res.*, 107, No. B4, doi:10.1029/2001JB000597.

Hirth, G., and D.L. Kohlstedt (1996) Water in the oceanic upper mantle: Implications for rheology, melt extraction and the evolution of the lithosphere. *Earth Planet. Sci. Lett.*, 144, 93–108.

Hofmeister, A.M. (1999) Mantle values of thermal conductivity and the geotherm from phonon lifetimes. *Science*, 283, 1699–1706.

Hofmeister, A.M., and R.E. Criss (2005) Earth's heat flux revised and linked to chemistry. *Tectonophysics*, 395, 159–177.

Jarvis, G.T. (1993) Effects of curvature in two-dimensional models of mantle convection: Cylindrical polar coordinates. *J. Geophys. Res.*, 98, 4477–4486.

Jellinek, A.M., R.C. Kerr, and R.W. Griffiths (1999) Mixing and compositional stratification produced by natural convection I. Experiments and their application to Earth's core and mantle. *J. Geophys. Res.*, 104(B4), 7183–7201.

Kameyama, M., D.A. Yuen, and S. Karato (1999) Thermal-mechanical effects of low-temperature plasticity (the Peierls mechanism) on the deformation of a viscoelastic shear zone. *Earth Planet. Sci.*, 168, 159–172.

Kameyama, M., A. Kageyama, and T. Sato (2005) Multigrid iterative algorithm using pseudo-compressibility for three-dimensional mantle convection with strongly variable viscosity. *J. Comput. Phys.*, 206, 162–181.

Kameyama, M. (2005) ACuTEMan: A multigrid-based mantle convection simulation code and its optimization to the Earth Simulator. *J. Earth Sim.*, 4, 2–10.

Kanda, R.V.S., and D.J. Stevenson (2006) Suction mechanism for iron entrainment into the lower mantle. *Geophys. Res. Lett.*, 33(2), L02310, doi:10.1029/200GL025009.

Katsura, T. et al. (2005) Precise determination of thermal expansion coefficient of MgSiO3 perovskite at the top of the lower mantle conditions, In Third Workshop on Earth's Mantle, Composition, Structure and Phase Transitions, Saint Malo, France.

Kido, M., and O. Cadek (1997) Inferences of viscosity from the oceanic geoid: Indication of a low viscosity zone below the 660-km discontinuity. *Earth Planet. Sci. Lett.*, 151, 125–138.

Korenaga, J. (2005) Firm mantle plumes and the nature of the core-mantle region. *Earth Planet. Sci. Lett.*, 232, 29–37.

Leitch, A.M., and D.A. Yuen (1989) Internal heating and thermal constraints on the mantle. *Geophys. Res. Lett.*, 16, 1407–1410.

Li, X.D., and B. Romanowicz (1996) Global mantle shear-velocity model developed using nonlinear asymptotic coupling theory. *Geophys. J. R. Astr. Soc.*, 101, 22245–22272.

Lin, J.-F. et al. (2005) Spin transition of iron in magnesiowüstite in the Earth's lower mantle. *Nature*, 436, 377–380.

Machetel, P., and P. Weber (1991) Intermittent layered convection in a model mantle with an endothermic phase change at 670 km. *Nature*, 350, 55–57.

Manga, M., and R. Jeanloz (1996) Implications of a metal-bearing chemical boundary layer in D″ for mantle dynamics. *Geophys. Res. Lett.*, 23(22), 3091–3094.

Maruyama, S. (1994) Plume tectonics. *J. Geol. Soc. Jpn.*, 100(1), 25–49.

Masters, G., G. Laske, H. Bolton, and A. Dziewonski (2000) The relative behavior of shear velocity, bulk sound speed and compressional velocity in the mantle: Implications for chemical and thermal structure. In Karato, S., A.M. Forte, R.C. Liebermann, G. Masters, and L. Stixrude (eds.) Earth's Deep Interior, A.G.U. Monograph, 117, A.G.U., Washington, D.C., pp. 63–87.

Matyska, C., J. Moser, and D.A. Yuen (1994) The potential influence of radiative heat transfer on the formation of megaplumes in the lower mantle. *Earth Planet. Sci. Lett.*, 125, 255–266, 1994.

Matyska, C., and D.A. Yuen (2005) The importance of radiative heat transfer on superplumes in the lower mantle with the new post-perovskite phase change. *Earth Planet. Sci. Lett.*, 234, 71–81.

Matyska, C., and D.A. Yuen (2006) Lower mantle dynamics with the post-perovskite phase change, radiative thermal conductivity, temperature- and depth-dependent viscosity. *Phys. Earth Planet. Inter.*, 154, 196–207.

Matyska, C., and D.A. Yuen (2007) Upper-mantle versus lower-mantle plumes: Are they the same? In press, Foulger G., and D.M. Jurdy (eds.) The Origin of Melting Anomalies: Plumes, Plates and Planetary Processes, Geological Society of America.

Mc Namara, A.K., and S. Zhong (2004) Thermochemical structures within a spherical mantle: Superplumes or piles? *J. Geophys. Res.*, 109, B07402, doi:10.1029/2003JB002847.

McNutt, M., and A. Judge (1990) The superswell and mantle dynamics beneath the South Pacific. *Science*, 248, 969–975.

Mitrovica, J.X., and A.M. Forte (2004) A new inference of mantle viscosity based upon joint inversion of convection and glacial isostatic adjustment data. *Earth Planet. Sci. Lett.*, 225, 177–189.

Mittelstädt, E., and P.J. Tackley (2006) Plume heat flow is much lower than CMB heat flow. *Earth Planet. Sci. Lett.*, 241, 201–210.

Monnereau, M., and M. Rabinowicz (1996) Is the 670 km phase transition able to layer the Earth's convection in a mantle with depth-dependent viscosity? *Geophys. Res. Lett.*, 23, 1001–1004.

Monnereau, M., and D.A. Yuen (2002) How flat is the lower-mantle temperature gradient? *Earth Planet. Sci. Lett.*, 202, 171–183.

Montelli, R., G. Nolet, F.A. Dahlen, G. Masters, E.R. Engdahl and S.-H. Hung (2004) Finite-frequency tomography reveals a variety of plumes in the mantle. *Science*, 303, 338–343.

Morgan, W.J. (1971) Convection plumes in the lower mantle. *Nature*, 230, 42–43.

Moser, J., D.A. Yuen, T.B. Larsen, and C. Matyska (1997) Dynamical influences of depth-dependent properties on mantle upwellings and temporal variations of the moment of inertia. *Phys. Earth Plan. Inter.*, 102, 153–170.

Mühlhaus, H.B., and K. Regenauer-Lieb (2005) Towards a self-consistent plate mantle model that includes elasticity: Simple benchmarks and application to basic modes of convection. *Geophys. J. Int.*, 163, 788–800.

Murakami, M., K. Hirose, K. Kawamura, N. Sata, and Y. Ohishi (2004) Post-perovskite phase transition in MgSiO3. *Science*, 304, 855–858.

Nakagawa, T. and P.J. Tackley (2004a) Effects of a perovskite-post perovskite phase transition near core-mantle boundary in compressible mantle convection. *Geophys. Res. Lett.*, 31, L16611, doi:10.1029/2004GL020648.

Nakagawa, T., and P.J. Tackley (2004b) Effects of thermal-chemical mantle convection on the thermal evolution of the Earth's cores. *Earth Planet. Sci. Lett.*, 220, 107–119.

Ni, S., and D.V. Helmberger (2003) Ridge-like lower mantle structure beneath South Africa. *J. Geophys. Res.*, 108, B2, doi:10.1029/2001JB001545.

Oganov, A.R., and S. Ono (2004) Theoretical and experimental evidence for a postperovskite phase of MgSiO3 in Earth's D″ layer. *Nature*, 430, 445–448.

Petford, N., D.A. Yuen, T. Rushmer, J. Brodholt, and S. Stackhouse (2005) Shear-induced material transfer across the core-mantle boundary aided by the post-perovskite phase transition. *Earth Planet Space*, 57, 459–464.

Ranalli, G. (1995) Rheology of the Earth, 2nd Edition, 413pp, Cambridge Univ. Press.

Regenauer-Lieb, K., and D.A. Yuen (2003) Modeling shear zones in geological and planetary sciences: Solid- and fluid-thermal-mechanical approaches. *Earth Sci. Rev.*, 63(3), 295–349.

Ricard, Y., L. Fleitout, and C. Froidevaux (1984) Geoid heights and lithospheric stresses for a dynamic earth. *Ann. Geophys.*, 2, 267–286.

Ricard, Y., and B. Wuming (1991) Inferring viscosity and the 3-D density structure of the mantle from geoid, topography and plate velocities. *Geophys. J. Int.*, 105, 561–572.

Richter, F.M., and B.E. Parsons (1975) On the interaction of two scales of convection in the mantle. *J. Geophys. Res.*, 80, 2529–2541.

Sammis, C.G., J.C. Smith, G. Schubert, and D.A. Yuen (1977) Viscosity-depth profile in the Earth's mantle: Effects of polymorphic phase transitions. *J. Geophys. Res.*, 85, 3747–3761.

Schott, B., D.A. Yuen, and A. Braun (2002) The influences of compositional and temperature-dependent rheology in thermal-chemical convection on entrainment of the D″-layer. *Phys. Earth Planet. Inter.*, 129, 43–65.

Schubert, G., D. Bercovici, and G.A. Glatzmaier (1990) Mantle dynamics in Mars and Venus: Influence of an immobile lithosphere on three-dimensional mantle convection. *J. Geophys. Res.*, 95, 14105–14129.

Schubert, G., D.L. Turcotte, and P.L. Olson (2001) Mantle Convection in the Earth and Planets, Chapter 6, Cambridge Univ. Press.

Schubert, G., G. Masters, P. Olson, and P.J. Tackley (2004) Superplumes or plume clusters? *Phys. Earth Planet. Inter.*, 146, 147–162.

Solomatov, V. (1996) Can hotter mantle have a larger viscosity? *Geophys. Res. Lett.*, 23, 937–940.

Speziale, S., A. Milner, V.E. Lee, S.M. Clark, M.P. Pasternak, and R. Jeanloz (2005) Iron spin transition in Earth's mantle. *Proc. National Academy Sci. USA*, 102(50), 17918–17922.

Steinbach, V., and D.A. Yuen (1994) Melting instabilities in the transition zone. *Earth Planet. Sci. Lett.*, 127, 67–75.

Steinbach, V., and D.A. Yuen (1998) The influences of surface temperature on upwellings in planetary convection with phase transitions. *Earth Planet. Sci. Lett.*, 162, 15–25.

Su, W.-J., and A. Dziewonski (1992) On the scale of mantle heterogeneity. *Phys. Earth Planet. Inter.*, 74, 29–54.

Tackley, P.J. (1996) Effects of strongly variable viscosity on three-dimensional compressible convection in planetary mantles. *J. Geophys. Res.*, 101, 3311–3332.

Tackley, P.J. (1998) Three-dimensional simulations of mantle convection with a thermo-chemical CMB boundary layer: D″. In Gurnis, M., M. Wysession, and E. Knittle (eds.) The Core-Mantle Boundary Region, American Geophysical Union, Washington D.C., pp. 231–253.

Tackley, P.J. (2002) Strong heterogeneity caused by deep mantle layering. *Geochem. Geophys. Geosyst.*, 3(4), 1, CiteID 1024, doi:10.1029/2001GC000167.

Tan, E., and M. Gurnis (2005) Metastable superplumes and mantle compressibility. *Geophys. Res. Lett.*, 32, L20307, doi:10.1029/2005GL024190.

Trampert, J., F. Deschamps, J. Resovsky, and D.A. Yuen (2004) Probabilistic tomography maps chemical heterogeneities throughout the lower mantle. *Science*, 306, 853–856.

Trompert, R., and U. Hansen (1998) Mantle convection simulations with rheologies that generate plate-like behavior. *Nature*, 395, 686–689.

Tsuchiya, T., J. Tsuchiya, K. Umemoto, and R.M. Wentzcovitch (2004) Phase transition in MgSiO3 perovskite in the lower mantle. *Earth Planet. Sci. Lett.*, 224, 241–248.

Tsuchiya, T., R.M. Wentzcovitch, C.R.S. da Silva, and S. de Gironcoli (2006) Spin transition in magnesiowüstite in Earth's lower mantle. *Phys. Rev. Lett.*, 96,198501.

Van den Berg, A.P., and D.A. Yuen (1998) Modeling planetary dynamics by using the temperature at the core-mantle boundary as a control variable. *Phys. Earth Planet. Inter.*, 108, 219–234.

Van Keken, P.E., and D.A. Yuen (1995) Dynamical influences of high viscosity in the lower mantle induced by the steep melting curve of perovskite: Effects of curvature and time dependence. *J. Geophys. Res.*, 100, 15233–15248.

Vincent, A.P., and D.A. Yuen (1988) Thermal attractor in chaotic convection with high Prandtl number fluids. *Phys. Rev. A*, 38, 328–334.

Walzer, U., R. Handel, and J. Baumgardner (2004) The effects of a variation of the radial viscosity profile on mantle evolution, *Tectonophysics*, 384, 55–90.

Whitehead, J.A., and B. Parsons (1978) Observations of convection at Rayleigh numbers up to 760,000 in a fluid with large Prandtl number. *Geophys. Astrophys. Fluid Dyn.*, 9, 201–217.

Yanagawa, T.K.B., M. Nakada, and D.A. Yuen (2005) Influence of lattice thermal conductivity on thermal convection with strongly temperature-dependent viscosity. *Earth Planets Space*, 57, 15–28.

Yoshida, M., and M. Ogawa (2004) Influence of two major phase transitions on mantle convection with moving and subducting plates. *Earth Planets Space*, 56, 1019–1033.

Yoshida, M., and A. Kageyama (2006) Low-degree mantle convection with strongly temperature- and depth-dependent viscosity in a three-dimensional spherical shell. *J. Geophys. Res.*, 111, B03412, doi:10.1029/2005JB003905.

Yuen, D.A., and W.R. Peltier (1980) Mantle plumes and the thermal stability of the D″ layer. *Geophys. Res. Lett.*, 7, 625–628.

Yuen, D.A., O. Cadek, A. Chopelas, and C. Matyska (1993) Geophysical inferences of thermal-chemical structures in the lower mantle. *Geophys. Res. Lett.*, 20, 889–902.

Yuen, D.A., O. Cadek, P. van Keken, D.M. Reuteler, H. Kyvalova, and B.A. Schroeder (1996) Combined results for mineral physics, tomography and mantle convection and their implications on global geodynamics. In Boschi, E., G. Ekstrom, and A. Morelli (eds.) Seismic Modelling of the Earth's Structure, Editrice Compositori, Bologna, Italy, pp. 463–506.

Zhang, S., and D.A. Yuen (1995) The influences of lower-mantle viscosity stratification on 3-D spherical-shell mantle convection. *Earth Planet. Sci. Lett.*, 132, 157–166.

Zhang, S., and D.A. Yuen (1996) Various influences on plumes and dynamics in time-dependent, compressible, mantle convection in 3-D spherical shell. *Phys. Earth Planet. Inter.*, 94, 241–267.

Zhao, D. (2001) Seismic structure and origin of hotspots and mantle plume. *Earth Planet. Sci. Lett.*, 192, 251–265.

Zhao, D. (2004) Global tomographic images of mantle plumes and subducting slabs: Insight into deep Earth dynamics. *Phys. Earth Planet. Inter.*, 146, 3–34.

Zhong, S., M.T. Zuber, L. Moresi, and M. Gurnis (2000) Role of temperature-dependent viscosity and surface plates in spherical shell models of mantle convection. *J. Geophys. Res.*, 105(B5), 11063–11082.